Gallium(III) and Iron(III) Complexes of α-N-Heterocyclic Thiosemicarbazones: Synthesis, Characterization, Cytotoxicity, and Interaction with Ribonucleotide Reductase

Christian R. Kowol,[†] Roland Berger,[†] Rene Eichinger,[†] Alexander Roller,[†] Michael A. Jakupec,[†] Peter P. Schmidt,[#] Vladimir B. Arion,*[,†] and Bernhard K. Keppler*[,†]

Institute of Inorganic Chemistry, Faculty of Chemistry, University of Vienna, Waehringer Strasse 42, A-1090 Vienna, Austria, and Max-Planck Institute for Bioinorganic Chemistry, Stiftstrasse 34-38, Mülheim an der Ruhr, D-45470 Germany

Received October 28, 2006

A series of gallium(III) and iron(III) complexes with five different [4]N-substituted α-N-heterocyclic thiosemicarbazones, viz., 2-acetylpyridine *N*,*N*-dimethylthiosemicarbazone (**1**), 2-acetylpyridine *N*-pyrrolidinylthiosemicarbazone (**2**), acetylpyrazine *N*,*N*-dimethylthiosemicarbazone (**3**), acetylpyrazine *N*-pyrrolidinylthiosemicarbazone (**4**), and acetylpyrazine *N*-piperidinylthiosemicarbazone (**5**), with the general formula $[GaLCl_2]$ (HL = **1** and **2**) and $[ML_2][Y]$ (M = Ga, HL = **1**−**5**, Y = PF_6; M = Fe, HL = **1**−**5**, Y = $FeCl_4$ and PF_6) were synthesized and characterized by elemental analysis, a number of spectroscopic methods (NMR, IR, UV−vis), mass spectrometry, and X-ray crystallography. The *in vitro* antitumor potency was studied in two human cancer cell lines (41M and SK-BR-3). The central metal ions exert pronounced effects in a divergent manner: gallium(III) enhances, whereas iron(III) weakens the cytotoxicity of the ligands. The capacity of ligand **1** and its Ga(III) and Fe(III) complexes to destroy the tyrosyl radical of the presumed target ribonucleotide reductase is reported.

Introduction

α-N-Heterocyclic thiosemicarbazones have been explored for their applicability as antitumor agents for half a century.[1] Their pharmacological potential has been recognized to include also antiviral, antimycobacterial, antifungal, and antimalarial properties,[2] and the enzyme ribonucleotide reductase has been identified as the principal target.[3−6] In fact, they are the strongest known inhibitors of this enzyme, both in cell-free assays and in intact tumor cells, being several orders of magnitude more effective than hydroxyurea, the first clinically applied ribonucleotide reductase inhibitor.[7,8] The enzyme that catalyzes the conversion of ribonucleotides to deoxyribonucleotides is produced at the transition from the G_1 to the S phase of the cell cycle as a prerequisite for DNA replication and is highly expressed in tumor cells, making it a suitable and well-established target for cancer chemotherapy. Mammalian (class Ia) ribonucleotide reductase is composed of an α_2 homodimer (R1 subunit) that contains the catalytically active center consisting of redox-active cysteines that are regenerated by the action of thioredoxin and a β_2 homodimer (R2 subunit) containing a tyrosyl radical and a diiron center which are essential for initiation of the nucleotide reduction process at the active site in R1.[9] Inhibitors of this enzyme are classified by their mode of interference with the enzyme's functions: (i) radical scavengers (e.g., hydroxyurea) that destroy the tyrosyl radical directly; (ii) chelating molecules (e.g., desferrioxamine) that remove iron from or prevent incorporation of iron into the metal binding site thereby quenching the tyrosyl radical indirectly or inhibiting its formation, and (iii) nucleotide and nucleoside analogues (e.g., gemcitabine, cladribine, fludarabine, cytarabine) that interfere with substrate binding.

The ribonucleotide reductase-inhibiting activity of α-N-heterocyclic thiosemicarbazones has primarily been explained by their iron-chelating properties, either by coordination of iron from the R2 subunit or by preformation of an iron chelate which then inhibits the enzyme, implying that iron complexes might actually be the active species. The observation that the preformed iron chelates are more potent inhibitors of ribonucleotide reductase in the absence of additional iron than the uncomplexed thiosemicarbazones supports the latter hypothesis, but any interaction restricted to the iron site of the enzyme is unable to explain the partially protective effects observed with thioredoxin and small dithiol compounds.[6,10,11] It was then proposed that preformed iron(III) chelates are readily reduced in blood or in the presence of thiols to the ferrous form[11−13] which is able to destroy the tyrosyl radical of the enzyme by a one-electron reduction in an oxygen-requiring reaction.[14] The assumption that the activity of α-N-heterocyclic thiosemicarbazones is not solely based on their iron-chelating properties has recently found support in the observation that 3-aminopyridine-2-carboxaldehyde-thiosemicarbazone (3-AP, triapine) induces iron-dependent free radical damage, thereby behaving distinctly different from classic iron-chelating drugs such as desferrioxamine.[15]

Apart from the well-established inhibition of ribonucleotide reductase, additional targets and modes of action have also been discussed. In particular, radical reactions similar to those induced by bleomycin may explain the formation of DNA strand breaks observed with 5-hydroxy-2-formylpyridine-thiosemicarbazone (5-HP)[16] and 1-formylisoquinoline-thiosemicarbazone,[17] suggesting the induction of direct DNA damage that might be reinforced by the inhibitory effects on ribonucleotide reductase.[7] Besides, inhibition of topoisomerase II by a mechanism distinctly different from that of etoposide has been suggested for a variety of [4]N-substituted thiosemicarbazones and, in particular, their copper(II) complexes.[18−20]

The major problem encountered in the development of α-N-heterocyclic thiosemicarbazones is the high general toxicity and, consequently, the low therapeutic index of many representatives of this class of compounds. Apart from its rapid inactivation by glucoronidation, 5-hydroxy-2-formylpyridine-thiosemicar-

* To whom correspondence should be addressed. Phone: +431427752600. Fax: +431427752680. E-mail: vladimir.arion@univie.ac.at; bernhard.keppler@univie.ac.at.
[†] University of Vienna.
[#] Max-Planck Institute for Bioinorganic Chemistry.

10.1021/jm0612618 CCC: $37.00
Published on Web 02/22/2007

bazone, the first clinically evaluated representative, had been withdrawn because of severe hematological and gastrointestinal side effects.[21,22] More recently, however, triapine has entered the clinical stage of development.[23−26] This compound shows therapeutic activity over a certain range of dosages in preclinical tumor models without imposing intolerable host toxicity[27] and has led to a renewed interest in this class of compounds.

The rationale for preparing gallium(III) complexes of α-N-heterocyclic thiosemicarbazones is based on the fact that gallium(III) also inhibits the activity of ribonucleotide reductase[28] and is endowed with clinically useful antiproliferative properties.[29−31] Due to similarity in ligand binding affinity with iron(III), gallium(III) affects intracellular iron availability, but also interacts directly with ribonucleotide reductase, by competing with iron for its binding site in the R2 subunit of the enzyme.[32,33] Combining a central metal and a ligand that are directed at the same molecular target in different ways is being pursued as a strategy to produce highly potent ribonucleotide reductase inhibitors expected to benefit from a synergistic action of the two components.

A prototypic, highly cytotoxic gallium complex with 2-acetylpyridine *N*,*N*-dimethylthiosemicarbazone has been reported recently.[34] The concentration−effect curves of this complex closely parallel those of the uncomplexed thiosemicarbazone, indicating that the cytotoxic properties of the complex are largely governed by the ligand. However, an increase in cytotoxic potency gained by complexation with gallium has been observed. This seemed to be explainable by the metal-to-ligand stoichiometry of 1:2, raising the question whether gallium(III) specifically contributes to the biological activity or whether similar effects might be achieved by complexation to iron. Furthermore, structural rearrangements in solution have been recognized in the case of this complex, resulting in a mixture of species with 1:2 and 1:1 metal-to-ligand stoichiometry, complicating the interpretation of the biological results obtained with this compound.

The aim of the present study was the synthesis of a series of related α-N-heterocyclic thiosemicarbazone complexes allowing the exploration of structure−activity relationships with regard to the role of the central metal (gallium vs iron), the metal-to-ligand stoichiometry, and the impact of structural modifications of the thiosemicarbazone ligand.

Results and Discussion

Syntheses. Complex **6** (Figure 1) with metal-to-ligand stoichiometry 1:1 ($[GaLCl_2]$) has been obtained from **1** and $GaCl_3$ in a 2:1 molar ratio in boiling dry ethanol in 68% yield, whereas the synthesis of **7** has been performed starting from **2** and $GaCl_3$ in 1:2 molar ratio with 82% yield. The formation of **6** and **7** has been corroborated by elemental analyses and electron impact (EI) mass spectra. The latter showed the presence of intense molecular ion peaks at *m*/*z* 360 with relative intensity (r.i.) 53.7% for **6** and 386 (r.i. 98.4%) for **7**. Other signals observed (see Supporting Information) could easily be related to structural fragments emerging from molecular ions M^+. It should also be noted that electrospray ionization (ESI) did not provide ions that could be related to the structures of **6** and **7**. Starting from $Ga(NO_3)_3$ and the corresponding ligands **1**−**5** in 1:2 molar ratio in ethanol by subsequent addition of NH_4PF_6, complexes $[GaL_2]^+$ (**8**−**12**) have been isolated as hexafluorophosphates in 56−91% yield. Complexes **13**−**15** have been produced by reacting $FeCl_3$ with the corresponding ligand in 1:1 molar ratio in boiling dry ethanol, and complexes **16** and **17** in 3:2 molar ratio, respectively. The reaction of $Fe(NO_3)_3 \cdot 9H_2O$ with the ligands **1**−**5** in 1:2 molar ratio, followed by addition of an excess of hexafluorophosphate, produced complexes **18**−**22** in 72−92% yield. The positive ion ESI mass spectra of **8**−**12** and **13**−**22** showed strong peaks (see Supporting Information) due to $[GaL_2]^+$ (L = L^1−L^5) and $[FeL_2]^+$ (L = L^1−L^5), correspondingly. The presence of counterions PF_6^- or $[FeCl_4]^-$ has been proved by ESI mass spectra recorded in the negative ion mode. The electronic spectra of both gallium(III) and iron(III) complexes are dominated by intraligand transitions associated with pyridine or pyrazine ring, azomethine, and thione portions of the thiosemicarbazone moiety (see Supporting Information). Of note is the large increase in the magnitude of the band at ∼400 nm, which is assumed to originate from the thioamide portion of the thiosemicarbazone HL, upon complexation (Figure S1). The high intensity of this band of the ligand in the complexed form is expected on the basis of reduced symmetry and in addition due to the increased lengths of the chromophore along the axis of the molecule in the complex (trans-configuration) when compared to the metal-free ligand, which usually adopts cis-configuration. The d−d band with the maximum at 894 nm (**18**) and 957 nm (**15**), respectively, in the case of iron complexes is presumably due to $^2T_{2g} \rightarrow {}^2T_{1g}$ transition of the d^5 low-spin system.[35] Selected complexes **6**, **8**, **14**, and **18** were shown to be stable for at least 15 h when dissolved in a mixture of DMSO/H_2O 1:100 (v/v) (see Figures S1−S4). We also observed that more concentrated solution of **8** in DMSO/H_2O 1:1 (v/v) produced X-ray diffraction quality single crystals of the same composition as the starting material after 48 h (in line with UV/vis data).

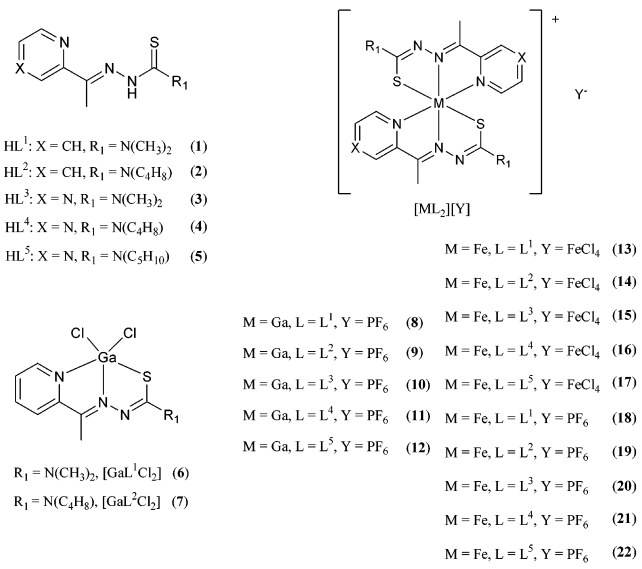

Figure 1. The library of thiosemicarbazones and their metal complexes.

All gallium and iron complexes were found to crystallize very well from chloroform or chloroform−ethanol mixtures saturated with hexane or diethyl ether. This enabled their characterization in the solid state by X-ray crystallography.

Crystal Structures. ORTEP drawings of $[Ga(L^1)Cl_2]$ (HL^1 = 2-acetylpyridine *N*,*N*-dimethylthiosemicarbazone) (**6**), the complex cation $[Ga(L^3)_2]^+$ (**10**), and $[Fe(L^3)_2]^+$ (**15**) (HL^3 = acetylpyrazine *N*,*N*-dimethylthiosemicarbazone) with the atom labeling schemes are shown in Figures 2 and 3, whereas those of complexes **11, 13, 16**−**18**, and **21** are quoted as Supporting Information (Figures S5−S10).

The geometry of the gallium ion in **6** is distorted square-pyramidal. The calculated τ value for the degree of trigonality is 0.28.[36] All compounds with metal-to-ligand stoichiometry

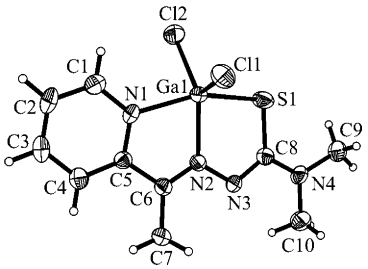

Figure 2. ORTEP drawing of $[GaL^1Cl_2]$ (HL^1 = 2-acetylpyridine *N*,*N*-dimethylthiosemicarbazone) (**6**) with thermal ellipsoids depicted at 50% probability level.

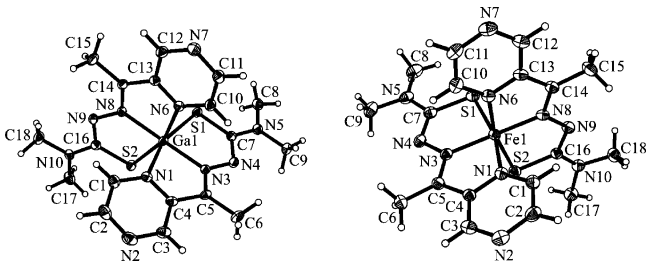

Figure 3. ORTEP drawing of the complex cations $[Ga(L^3)_2]^+$ (**10**) (left) and $[Fe(L^3)_2]^+$ (**15**) (right) (HL^3 = acetylpyrazine *N*,*N*-dimethylthiosemicarbazone) with thermal ellipsoids depicted at 50% probability level.

1:2 crystallize in centrosymmetric space groups as racemic mixtures of the two enantiomers of chiral octahedral gallium(III) or iron(III) complexes.

Cytotoxicity. The cytotoxic potencies of five ^{4}N-substituted α-N-heterocyclic thiosemicarbazones, seven gallium complexes, and ten iron complexes were investigated in the human tumor cell lines 41M (ovarian carcinoma) and SK-BR-3 (mammary carcinoma) by means of the colorimetric MTT assay. Generally, SK-BR-3 cells are less sensitive to the compounds investigated in this study, giving up to 38 times higher IC_{50} values than 41M cells. All the complexes and the ligands have very high cytotoxic potencies, with IC_{50} values ranging from picomolar to nanomolar concentrations (Table 1), and their concentration−effect curves are rather flat, gently declining over a range of 3 orders of magnitude (Figures 4−6), which contrasts with the steep concentration-effect curves usually observed with tumor-inhibiting metal compounds. This suggests that the cytotoxicity is mainly governed by the thiosemicarbazone ligands, which are highly cytotoxic themselves, while complexation to metal ions rather serves to modulate their mode of action and activity.

In order to give direction to the future development of this class of compounds, structure−activity relationships have been explored in following respects: (i) impact of complexation to gallium(III) or iron(III) as compared to the uncomplexed thiosemicarbazone; (ii) influence of the ligand-to-metal stoichiometry; (iii) structural modifications of the thiosemicarbazone and (iv) influence of the counterion in the iron(III) complex salts.

The effects of the central metal on the activity of ligands **1**−**5** are very pronounced, and notably they are divergent (Figure 4). Complexation to iron(III) weakens the cytotoxic properties to a remarkable extent. The IC_{50} values of the iron complexes range from 13 to 172 nM in the cell line 41M and from 29 to 930 nM in SK-BR-3 cells, indicating roughly 12- to 2400-fold (41M) and 9- to 660-fold (SK-BR-3) lower cytotoxicities than those of the corresponding metal-free ligands, respectively. In contrast, 1:2 gallium(III) complexes (**8**−**12**) show an increase in cytotoxicity compared to the corresponding metal-free ligands

Table 1. Cytotoxicity of α-N-Heterocyclic Thiosemicarbazones (**1**−**5**), Their Gallium(III) Complexes (**6**−**12**), Iron(III) Complexes (**13**−**22**), Cisplatin, $Ga(NO_3)_3$, $Fe(NO_3)_3$, and NH_4PF_6 in Two Human Cancer Cell Lines[a]

	IC_{50} (nM)	
compd	41M	SK-BR-3
	Ligands	
1	0.22 ± 0.14	2.7 ± 1.4
2	0.36 ± 0.07	3.1 ± 1.1
3	0.073 ± 0.005	1.4 ± 0.1
4	1.1 ± 0.4	5.0 ± 2.3
5	0.41 ± 0.03	2.2 ± 0.3
	Ga(III) Complexes	
6	0.19 ± 0.15	0.59 ± 0.27[b]
7	0.16 ± 0.07[b]	1.8 ± 0.2
8	0.053 ± 0.018[b]	0.56 ± 0.47[b]
9	0.18 ± 0.03[b]	0.52 ± 0.05[b]
10	0.0045 ± 0.0006[b]	0.17 ± 0.01[b]
11	0.065 ± 0.042[b]	0.47 ± 0.22[b]
12	0.27 ± 0.08[b]	0.79 ± 0.05[b]
	Fe(III) Complexes	
13	154 ± 10[b]	447 ± 63[b]
14	26 ± 7[b]	29 ± 12[b]
15	172 ± 24[b]	930 ± 206[b]
16	13 ± 9[b]	104 ± 37[b]
17	27 ± 6[b]	64 ± 24[b]
18	126 ± 32[b]	452 ± 36[b]
19	54 ± 25[b]	87 ± 11[b]
20	149 ± 20[b]	682 ± 267[b]
21	17 ± 8[b]	76 ± 11[b]
22	57 ± 22[b]	120 ± 22[b]
cisplatin	0.39 ± 0.07 μM	
$Ga(NO_3)_3$	70 ± 4 μM	>100 μM
$Fe(NO_3)_3$	>100 μM	>100 μM
NH_4PF_6	>100 μM	>100 μM

[a] 50% inhibitory concentrations in 41M and SK-BR-3 cells after exposure for 96 h in the MTT assay. Values are means ± standard deviations obtained from at least three independent experiments. [b] Different from corresponding uncomplexed thiosemicarbazone (compounds **1**−**5**) ($p \le 0.1$; Wilcoxon rank sum test).

by a factor of 1.5 to 17 for 41M cells and 3 to 11 for SK-BR-3 cells, respectively. This results in IC_{50} values in the low nanomolar or even in the picomolar range (0.0045−0.27 nM for 41M and 0.17−1.8 nM for SK-BR-3 cells). A pairwise comparison of the direct analogues $[Ga(L^{1-5})_2][PF_6]$ and $[Fe(L^{1-5})_2][PF_6]$ reveals that the gallium complexes are by a factor of 210 to 33000 (41M) and 150 to 4000 (SK-BR-3) more cytotoxic than the iron compounds, respectively.

Since structural rearrangements in solution, resulting in a mixture of species with 1:2 and 1:1 metal-to-ligand stoichiometry (eq 1), had been recognized in the case of [bis(2-acetylpyridine *N*,*N*-dimethylthiosemicarbazone)gallium(III)] tetrachlorogallate(III) and analogous compounds with tetrachlorogallate(III) as counteranion,[37] the complex salts with hexafluorophosphate have been prepared.

$$[GaL_2][GaCl_4] \leftrightarrow 2[GaLCl_2] \quad (1)$$

In order to examine the influence of the ligand-to-metal stoichiometry, the gallium(III) complexes of the general formula $[GaLCl_2]$, i.e., **6** and **7**, were hence compared with their $[GaL_2][PF_6]$ congeners **8** and **9**, respectively (Figure 5). The cytotoxicity of complexes with metal-to-ligand stoichiometry 1:1 is either similar (**6** in 41M cells and **7** in both cell lines) or up to 4.6 times higher (**6** in SK-BR-3 cells) than those of the corresponding uncomplexed thiosemicarbazones. Although the former compounds contain two more easily replaceable chloro ligands, when compared to tridentate thiosemicarbazones, which

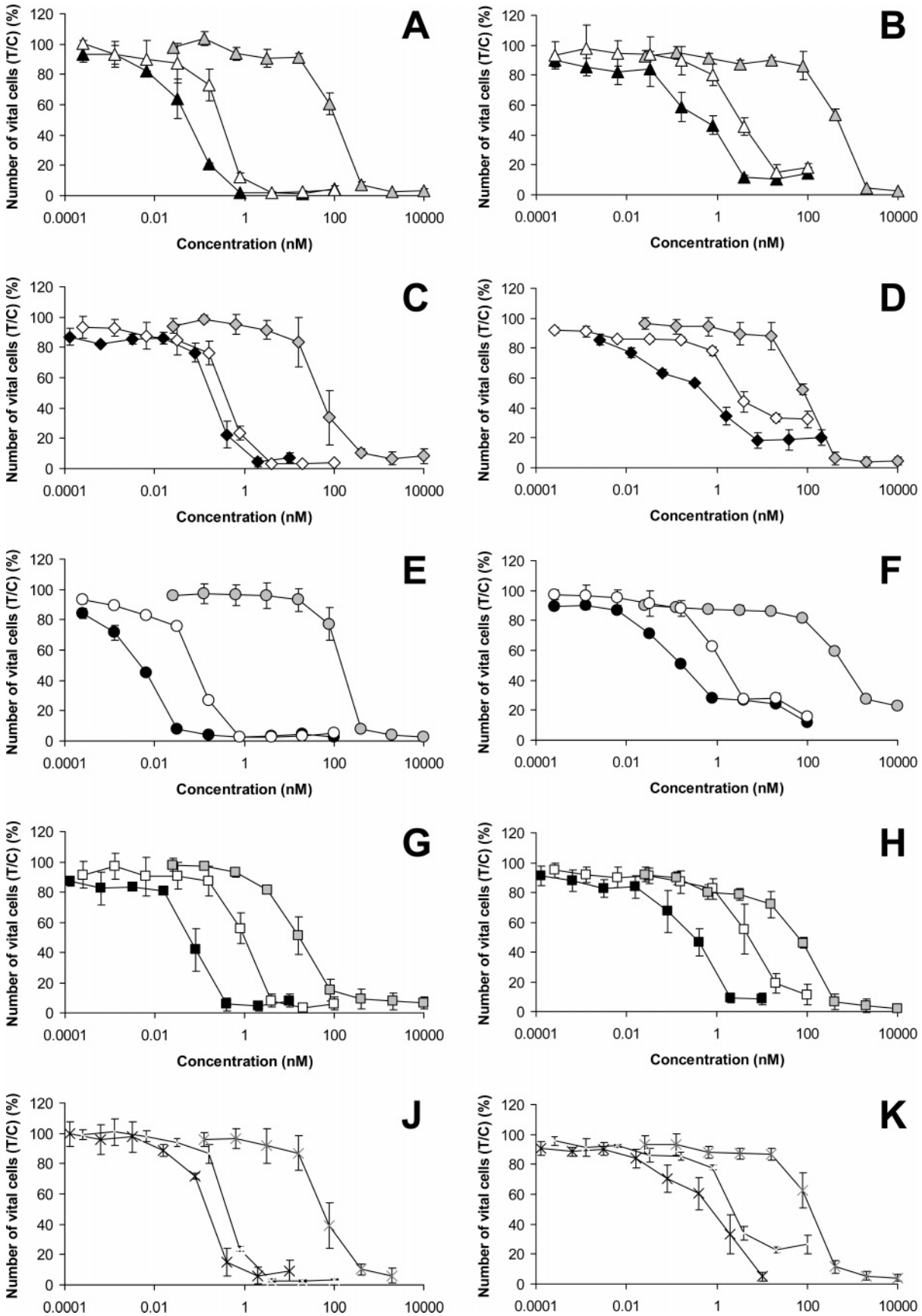

Figure 4. Concentration-effect curves of thiosemicarbazones HL (white symbols), their gallium(III) complexes $[GaL_2][PF_6]$ (black symbols), and iron(III) complexes $[FeL_2][PF_6]$ (gray symbols), obtained by the MTT assay in 41M cells (left panels: A, C, E, G, J) and SK-BR-3 cells (right panels: B, D, F, H, K). In each case, the thiosemicarbazone is less cytotoxic than the gallium complex, but more cytotoxic than the iron complex. A, B. Compounds **1** (white), **8** (black), and **18** (gray). C, D. Compounds **2** (white), **9** (black), and **19** (gray). E, F. Compounds **3** (white), **10** (black), and **20** (gray). G, H. Compounds **4** (white), **11** (black), and **21** (gray). J, K. Compounds **5** (white), **12** (black), and **22** (gray). Values are means ± standard deviations from at least three independent experiments.

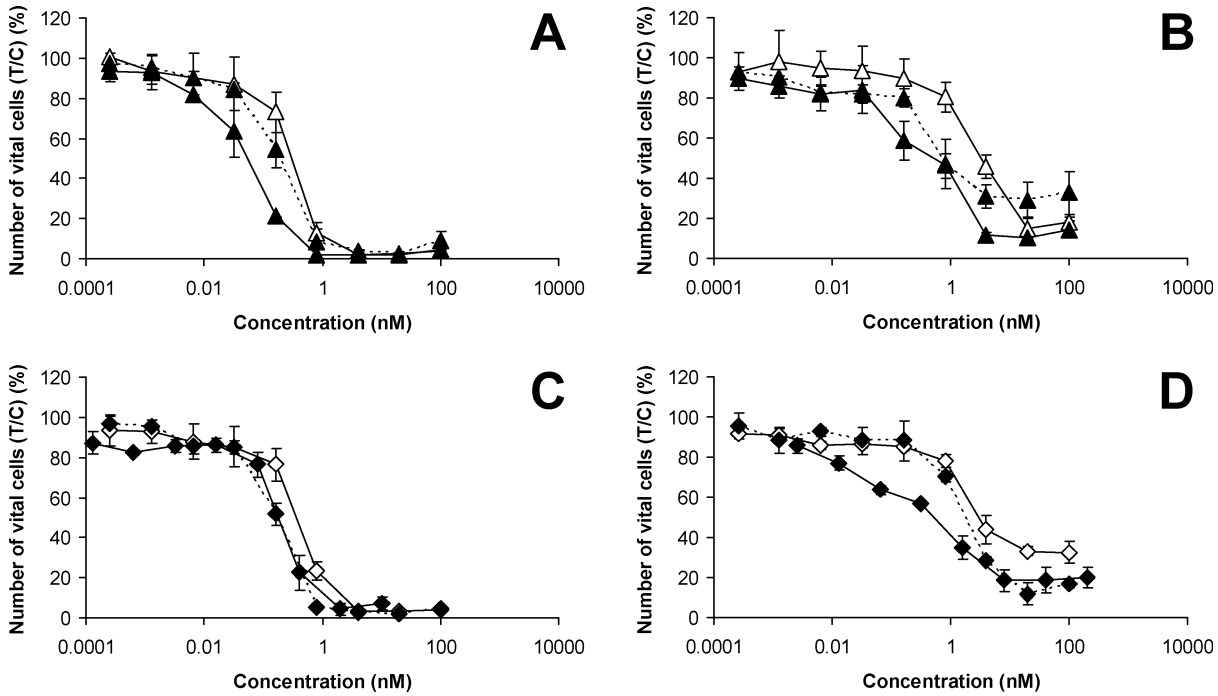

Figure 5. Concentration-effect curves of thiosemicarbazones HL (white symbols) and their gallium(III) complexes [$GaLCl_2$] (black symbols, dashed line) and [GaL_2][PF_6] (black symbols, solid line), obtained by the MTT assay in 41M cells (left panels: A, C) and SK-BR-3 cells (right panels: B, D). The complexes with metal-to-ligand stoichiometry 1:1 are at least as cytotoxic as the uncomplexed thiosemicarbazones but do not exceed their congeners with stoichiometry 1:2. A, B. Compounds **1** (white), **6** (black; dashed lines), and **8** (black; solid lines). C, D. Compounds **2** (white), **7** (black; dashed lines), and **9** (black; solid lines). Values are means ± standard deviations from at least three independent experiments.

should allow covalent binding to biomolecules more readily, neither the shapes of their concentration-effect curves nor their cytotoxic potencies suggest any substantial differences in their pharmacological behavior as compared to the congeners with stoichiometry 1:2.

Structural modifications of two moieties of the thiosemicarbazone ligands (aromatic N-heterocycle: pyridine vs pyrazine; terminal amine group: dimethylamine vs pyrrolidine vs piperidine) have been explored for their effect on the cytotoxicity of the complexes with 1:2 metal-to-ligand stoichiometry. For comparison, the concentration-effect curves of the uncomplexed thiosemicarbazones HL, i.e., **1**−**5**, the gallium(III) complexes [GaL_2][PF_6] **8**−**12**, and the iron(III) complexes [FeL_2][PF_6] **18**−**22** are depicted in Figure 6. In general, cytotoxic potencies mostly range within 1 order of magnitude for each class of compounds, and the effects exerted by the structural modifications of the thiosemicarbazone moieties are quite small in comparison to the impact of the central metal described above. Within the uncomplexed thiosemicarbazones, cytotoxicity decreases in the following rank order in both cell lines based on IC_{50} values: **3** > **1** ≈ **5** ≈ **2** > **4**.

Strikingly, the cytotoxicity-weakening effects of complexation with iron(III) become more pronounced with increasing cytotoxic potency of the thiosemicarbazone, resulting in an inverse rank order of the corresponding iron(III) complexes in 41M cells: **21** (ligand **4**) > **19** (ligand **2**) ≈ **22** (ligand **5**) > **18** (ligand **1**) ≥ **20** (ligand **3**). A similar tendency, though with a slightly deviating rank order, is discernible in SK-BR-3 cells. However, no structure−activity relationships with validity for both cell lines can be deduced from the concentration-effect curves of the gallium(III) complexes, and the rank orders with regard to cytoxic potency neither correspond to that of the uncomplexed thiosemicarbazones nor to that of the iron(III) analogues. Accordingly, there is no correlation between the cytotoxicity-enhancing effects of complexation with gallium(III) and the cytotoxic potency of the uncomplexed thiosemicarbazones.

The counterions of the cationic iron(III) complexes seem to have a marginal, if any, impact on cytotoxicity, as the differences between the IC_{50} values obtained with the complex salts containing either tetrachloroferrate(III) or hexafluorophosphate are mostly within the same range of variation.

Clarifying the question left open by a previous publication on the gallium(III) complex of 2-acetylpyridine *N*,*N*-dimethylthiosemicarbazone,[34] the work presented here clearly indicates that gallium(III) is able to enhance the cytotoxicity of α-N-heterocyclic thiosemicarbazones to an extent largely exceeding that of mere stoichiometric effects, whereas complexation to iron(III) is not only disadvantageous in comparison to gallium(III) but even results in a marked attenuation of the activity by 1 to 3 orders of magnitude. The latter observation deviates from findings reported in the literature for other α-N-heterocyclic thiosemicarbazones. On the one hand, it sharply contrasts with the enhancing effects of complexation with iron(III) on the cytotoxicity and the ribonucleotide reductase-inhibitory potency of 2-formylpyridine- and 1-formylisoquinoline-thiosemicarbazone[10] but also with the *in vivo* antileukemic behavior of a 2-acetylpyridine thiosemicarbazone analogue carrying a terminal hexahydroazepine group, which has been reported to be inactive unless complexed with iron(III).[38] On the other hand, the attenuating effects are much more pronounced than those reported for the complexation of ^{4}*N*-azabicyclononane-substituted thiosemicarbazones derived from 3-acetylpyridazine, 4-acetylpyrimidine, and acetylpyrazine with iron(II).[39] In consideration of the converse effects of iron(III) observed with the thiosemicarbazones studied here, the favorable properties obtained by complexation to gallium(III) can unequivocally and specifically be ascribed to this particular metal ion and are not the result of complexation in general or the

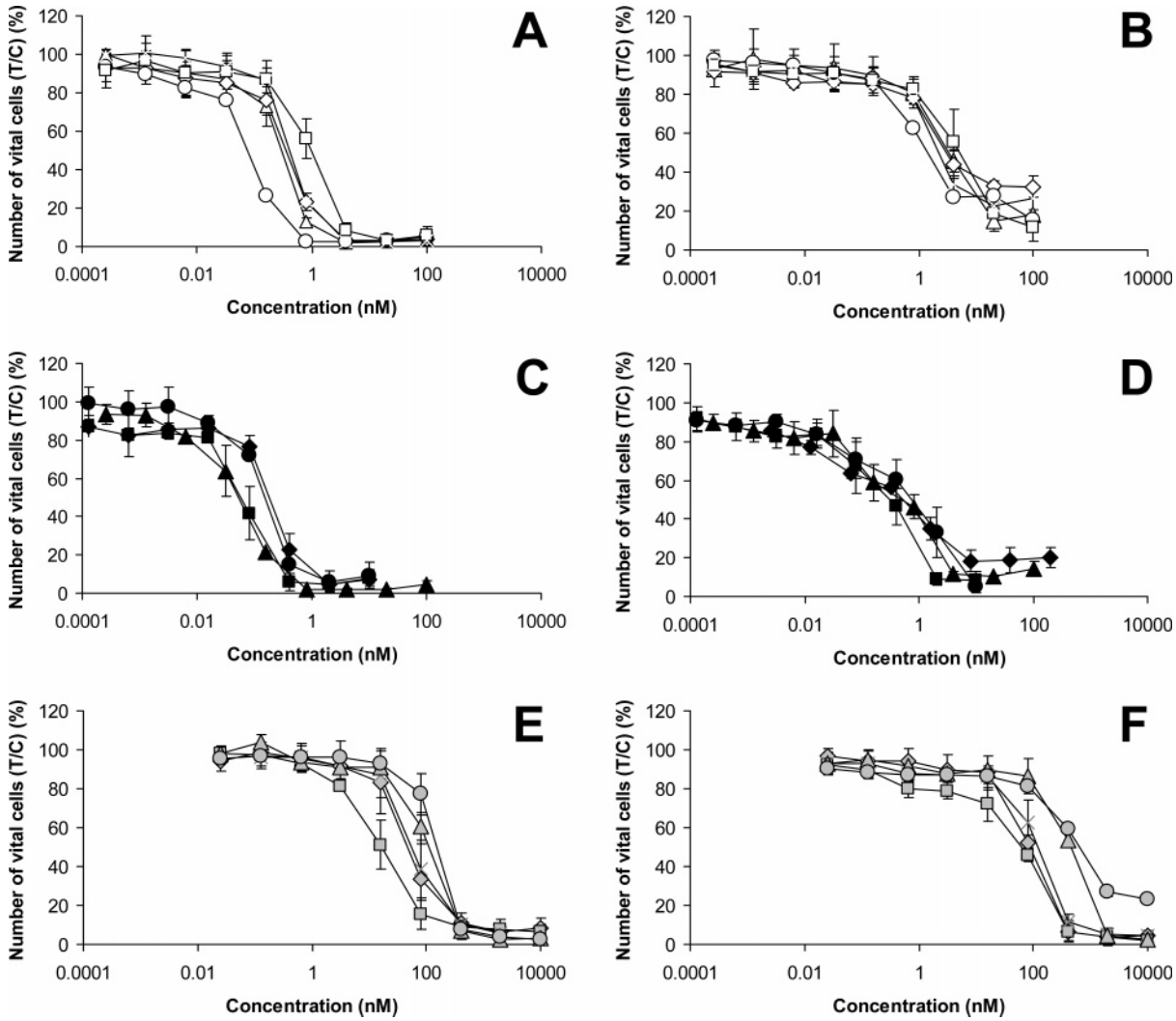

Figure 6. Concentration-effect curves of thiosemicarbazones HL (white symbols), their gallium(III) complexes $[GaL_2][PF_6]$ (black symbols) and iron(III) complexes $[FeL_2][PF_6]$ (gray symbols), obtained by the MTT assay in 41M cells (left panels: A, C, E) and SK−BR-3 cells (right panels: B, D, F). Within each class of compounds, cytotoxic potencies mostly range within 1 order of magnitude, and the structural modifications of the thiosemicarbazone moieties exert rather small effects in comparison to the impact of the central metal. A, B. Compounds **1** (−△−), **2** (−◇−), **3** (−○−), **4** (−□−) and **5** (−×−). C, D. Compounds **8** (−▲−), **9** (−◆−), **10** (−●−), **11** (−■−) and **12** (−×−). E, F. Compounds **18** (−▲−), **19** (−◆−), **20** (−●−), **21** (−■−) and **22** (−×−). Values are means ± standard deviations from at least three independent experiments.

geometry of the complex, which is essentially the same for both central metals (Figure 3).

These findings do not necessarily exclude the possibility that preformed iron chelates are the species actually exerting the biological effects *in vivo*, given the high affinity of the thiosemicarbazones for iron and the low concentrations of iron in cell culture media as compared to those encountered *in vivo*, but they clearly indicate that all thiosemicarbazones under investigation display their full antiproliferative potency when the metal-binding site is not occupied by iron. Whether the beneficial effects of coordination to gallium result from the pharmacological properties of this metal or from the fact that it prevents premature coordination to iron remains to be elucidated by further studies.

All five ligands used for synthesis of the complexes presented here are derived from a basic structure. As compared to the impact of complexation, the structural modifications of the thiosemicarbazones have comparatively little impact on their biological activity *in vitro*, suggesting that all thiosemicarbazone structures under investigation are capable of interacting with their common biological target in a comparable manner. The generally high cytotoxic potencies of compounds **1**−**5** are in accordance with literature data that report inhibition of lymphoma cell growth by compounds **1**, **3**, **4** and related ^{4}N-disubstituted α-N-heterocyclic thiosemicarbazones with IC_{50} values in the low nanomolar range.[40] When starting from the 2-acetylpyridine- or acetylpyrazine thiosemicarbazone structure, the dimethylation of the terminal nitrogen atom (^{4}N) of the thiosemicarbazone chain has been recognized as the crucial modification in order to obtain this exceptionally high cytotoxicity.[40] This tremendous cytotoxicity has been found to be preserved when the dimethylamino group is replaced by cycloamine functions (pyrrolidine or piperidine), which is also confirmed by the results presented here.

Whether the conclusions drawn from our *in vitro* findings, in particular the favorable effects of complexation with gallium(III), can be transferred to the *in vivo* setting is subject to ongoing studies in animal tumor models. As to the antitumor activity of the uncomplexed thiosemicarbazones, results reported in the literature are fragmentary and rather conflicting: In contrast to 2-formylpyridine-thiosemicarbazone,[1,5,41] 3-aminopyridine-2-carboxaldehyde thiosemicarbazone (3-AP, triapine)[42] and other representatives lacking substituents at the terminal amine nitrogen, 2-acetylpyridine *N*,*N*-dimethylthiosemicarba-

Table 2. Mouse R2 Tyrosyl Radical Concentration [Y*] in μM Measured under Aerobic and Anaerobic Conditions for Samples Containing 30 μM Reconstituted R2 Monomer and 30−33 μM Tested Compound after 1, 15, and 1005 min Total Incubation Time at 298 K

	tyrosyl radical concentration [Y*] in μM							
time[min]	blank	blank + DMSO	blank + DMSO + DTT	**$Ga(NO_3)_3$**	**$Fe(NO_3)_3$**	**1**	**8**	**18**
			Aerobic					
1			17.7	16.5	16.6	17.2	17.4	16.8
15			17.4	16.9	18.2	7.0	9.3	5.1
1005			5.9	5.4	0.9	0.5	0.3	0.6
			Anaerobic					
1	19.8	19.1	20.9	17.3	18.3	8.5	15.9	3.2
15	18	18.4	22.4	18.2	19.8	0	0	0
1005	2.6	3.2	0	0	0	0	0	0

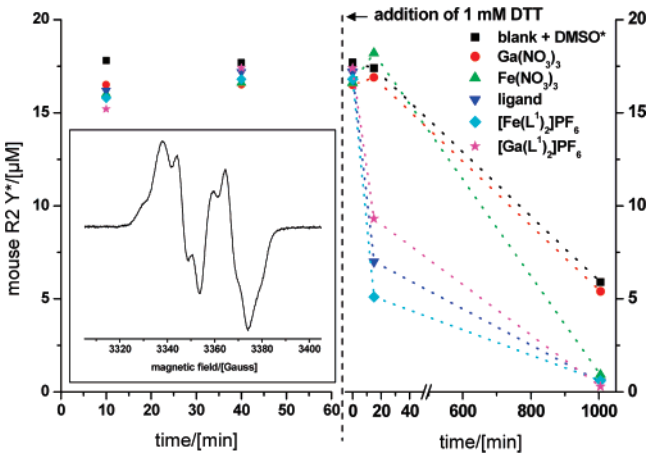

Figure 7. Mouse R2 tyrosyl radical concentration [Y*] in μM for samples containing 30 μM reconstituted R2 monomer and 33 μM tested compound after 10 and 40 min total incubation time at 298 K (left). Radical concentration [Y*] after addition of 1 mM DTT, measured after 1, 15, and 1005 min (right). Inset: X-band EPR spectrum of [Y*] of the blank at 40 K. Further EPR measuring conditions: 9.64 GHz, 100 kHz modulation frequency, 3 G modulation amplitude, 41 ms time constant, and 82 s recording time. *blank + DMSO (left) and blank + DMSO + DTT (right).

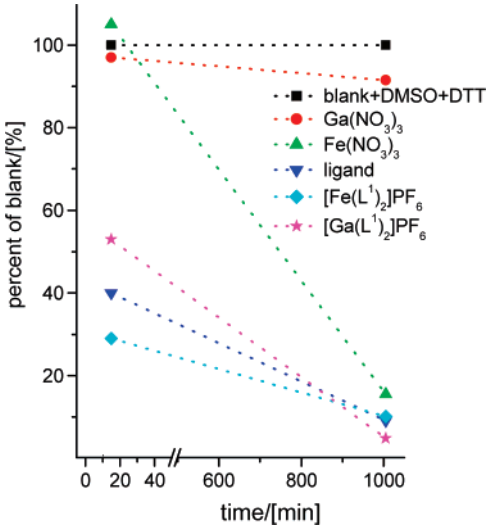

Figure 8. Percentage of the [Y*] concentrations in the samples from Figure 7 relating their Y* concentration to that of the blank, therefore accounting for the natural decay of the [Y*] concentration in mouse R2. Sample composition, incubation time, and conditions as in Figure 7.

zone is completely devoid of antileukemic activity in nontoxic doses in mice, whereas replacement of dimethylamine either by longer alkylamines or by bulky cycloamines results in restored activity, though at higher optimal doses,[43] suggesting that the introduction of a sterically more demanding substituent might be beneficial from a therapeutic point of view.

Interaction with Ribonucleotide Reductase. The sensitivity of the R2 specific tyrosine free radical in mouse ribonucleotide reductase R2 protein to 2-acetylpyridine *N*,*N*-dimethylthiosemicarbazone (**1**), its gallium(III) and iron(III) complexes $[Ga(L^1)_2][PF_6]$ (**8**) and $[Fe(L^1)_2][PF_6]$ (**18**), $Ga(NO_3)_3$, and $Fe(NO_3)_3$ was tested. A highly purified ribonucleotide reductase R2 protein (30 μM R2 monomer) in buffer containing 1% DMSO was incubated with 30−33 μM of the above-mentioned compounds along with the control sample (blank) for 10 min at 298 K. The frozen samples were analyzed by EPR spectroscopy, and the EPR spectra of the tyrosyl radical (Y*) were measured at 40 K. As the reaction time was short and the results after 10 min incubation time were not conclusive, the samples were thawed, and the compounds were allowed to react with ribonucleotide reductase R2 protein for further 30 min at 298 K. Measurement of the EPR spectra of the samples refrozen in liquid nitrogen showed no change of the EPR signal (Figure 7). The results obtained prompted us to investigate the same reaction in the presence of dithiothreitol (DTT) as a reductant. All six samples were thawed, and to each of them 1 mM (final concentration) of DTT was added. After incubation for 15 min, the samples were refrozen in liquid nitrogen and EPR spectra measured. As seen in Table 2 and Figure 7, the R2 specific EPR signal decreased significantly for HL^1, $[Ga(L^1)_2][PF_6]$, and $[Fe(L^1)_2][PF_6]$ but remained almost unchanged for $Ga(NO_3)_3$, $Fe(NO_3)_3$, and control experiment. The samples were thawed again, allowed to react for further 16 h at 298 K, and refrozen and the EPR spectra remeasured. All thiosemicarbazone-containing samples (**1**, **8**, and **18**) showed relatively fast kinetics for the destruction of the tyrosyl radical Y* (Figure 7). In comparison, Y* is slowly destroyed in the blank on the long time scale (>16 h), which is known from stability measurements. This decay is accounted for in Figure 8 by relating the Y* concentration of the samples to that of the blank in %, whereas in Figure 9 it is shown that 1% DMSO has no effect on the natural decay. Figure 8 shows clearly that $Ga(NO_3)_3$ does not enhance the decay of Y* in DTT-containing buffer under the experimental conditions and that $Fe(NO_3)_3$ displays a lag time in the destruction kinetics of Y* compared to the ligand-containing samples. These samples already exhibited after 15 min incubation time a quenching of Y* by more than 50%, whereas the $Fe(NO_3)_3$ sample still contained the same amount of Y* as the blank but shows a similar quenching of more than 80% after 16.5 h.

Under anaerobic conditions, the quenching of Y* by **1**, **8**, and **18** is much faster than in the presence of oxygen (Table 2 and Figure 9). In addition, the three species show very different reactivity with $[Fe(L^1)_2][PF_6] \gg$ ligand $\gg [Ga(L^1)_2][PF_6]$ under anaerobic conditions, whereas their aerobic reactivity displays only moderate differences, nevertheless, in the same order. However, quenching of Y* seems to be an insufficient explanation for antitumor potency because of the reversed order of the

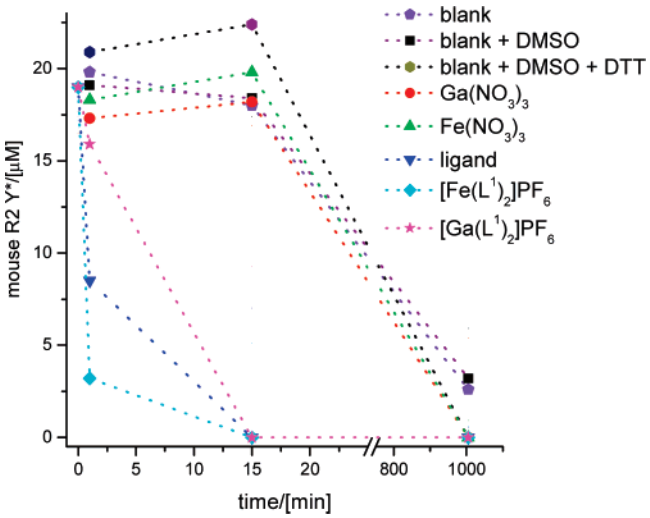

Figure 9. Mouse R2 tyrosyl radical concentration [Y*] in μM under anaerobic conditions for samples containing 30 μM reconstituted R2 monomer and 30 μM tested compound after 1, 15, and 1005 min total incubation time at 298 K. To underline that all samples had a similar starting concentration of [Y*] a virtual (not measured) starting data point at time 0 was included at the average [Y*] concentration of the other samples for the three ligand-containing samples displaying a fast Y* decay. EPR measuring conditions: 9.42 GHz and 77 K, all other settings as in Figure 7.

latter. This might suggest the existence of additional molecular targets less considered so far.

As for aerobic conditions, under anaerobic conditions the presence of DTT alone or with one of the metal nitrates shows no significant effect after 15 min incubation. However, the lack of oxygen in presence of DTT increases the instability of Y* also in the blank, so that it is decayed completely after 16.6 h incubation, preventing any conclusion on an additional reactivity of the two metal nitrates. This accelerated decay indicates that DTT acts as a slow radical quencher in the absence of oxygen. Surprisingly, Y* decays faster in the absence of DTT under anaerobic conditions than in presence of both oxygen and DTT, as can be seen from the Y* concentration of these blanks after 16.6 h in Figures 7 and 9. This together with the unexpected results from the anaerobic DTT containing blank and the aerobic $Fe(NO_3)_3$/DTT containing sample might be explained by reduction of Fe(III) to Fe(II) in the presence of DTT. Here, Fe(III) is available in mouse R2 solutions as R2 is isolated as Y*- and iron-free apoprotein and reconstituted with four Fe(II)/monomer[44] resulting in an optimal Y* yield of 0.7 ± 0.1 Y*/monomer. Although only two Fe(III) are bound tightly at the diiron binding site of each monomer, not more than 15% of the excess iron can be removed from the mouse R2 protein by, e.g., size exclusion chromatography.[45] Nevertheless, this excess Fe(III) most likely bound to the protein surface and the iron bound at the diiron binding site of R2 monomers, where no Y* has been formed, are available in solution[46] and might react with the DTT. During reconstitution, an Fe(II) is delivering an electron to the diiron-center-radical site from the surface of the R2 protein,[9,44] and in a similar way the delivery of an electron from bound Fe(II) to Y* in reconstituted R2 might quench the radical. This directly explains the faster radical decay in the anaerobic DTT containing blank. In the aerobic samples, formation of Fe(II) by DTT would initiate two counter-working reactions as the combination of Fe(II) and oxygen reconstitutes the tyrosyl radical again. The slower Y* decay in the DTT and oxygen containing blank (Figure 7) compared to the blank containing neither oxygen nor DTT (Figure 9) indicates that the reconstitution is more efficient. This in turn explains the result from the aerobic $Fe(NO_3)_3$/DTT-containing sample (Figure 7), in which the oxygen compensates the tyrosyl radical destruction in the first 15 min but is used up on the long time scale, where the quenching by Fe(II) prevails.

Conclusions

The combination of ^{4}N-substituted α-N-heterocyclic thiosemicarbazone moieties with a central gallium(III) ion, both well-known inhibitors of the enzyme ribonucleotide reductase, yielded a series of highly potent antiproliferative coordination compounds that are being explored for their applicability as anticancer agents. Although the pharmacological properties of these complexes must be primarily attributed to the thiosemicarbazone ligands, gallium(III) unequivocally and specifically modulates their cytotoxic potency in a beneficial way. In contrast, coordination to iron(III), which is most likely the principal biotransformation process undergone by α-N-heterocyclic thiosemicarbazones *in vivo*, actually impairs the biological activity of all representatives of this class of compounds investigated in this study. Although slow Y* quenching on the hour time scale has been found in DTT-containing mouse R2 solution without the thiosemicarbazone ligand, the much faster reaction on the minute time scale in presence of the ligand clearly shows that the Y* in mammalian R2 protein is a direct and preferred target of α-N-heterocyclic thiosemicarbazones under slightly reducing conditions, which also prevail in cancer cells. The reversed order of cytotoxic activity $[Ga(L^1)_2][PF_6]$ > HL^1 > $[Fe(L^1)_2][PF_6]$ and Y* quenching kinetics $[Fe(L^1)_2][PF_6]$ > HL^1 > $[Ga(L^1)_2][PF_6]$ nicely displays the difference between a complex whole cell and a purified protein solution. A number of explanations, starting from the uptake kinetics to additional reactions with target(s) other than ribonucleotide reductase, are imaginable for this solely quantitative difference.

Experimental Section

All solvents and reagents were obtained from commercial suppliers and used without further purification. 2-Acetylpyridine *N*,*N*-dimethylthiosemicarbazone (**1**), 2-acetylpyridine *N*-pyrrolidinylthiosemicarbazone (**2**), acetylpyrazine *N*,*N*-dimethylthiosemicarbazone (**3**), acetylpyrazine *N*-pyrrolidinylthiosemicarbazone (**4**), and acetylpyrazine *N*-piperidinylthiosemicarbazone (**5**) have been prepared as described in the literature.[40,47] Elemental analyses were carried out on a Carlo Erba microanalyzer at the Microanalytical Laboratory of the University of Vienna and were within ±0.4% of the theoretical values. Electrospray ionization mass spectrometry was carried out with a Bruker Esquire 3000 instrument (Bruker Daltonic, Bremen, Germany). Electron impact mass spectrometry was carried out at 70 eV with a Finnigan MAT 8230 (Bremen, Germany). Expected and experimental isotope distributions were compared. Infrared spectra were obtained from KBr or CsI pellets with a Perkin-Elmer FT-IR 2000 instrument (4000−200 cm^{-1}). UV−vis spectra were recorded on a Perkin-Elmer Lambda 650 UV−vis-spectrophotometer using samples dissolved in methanol (900−200 nm). **15** and **18** were also measured on a Hewlett-Packard 8453 UV−vis spectrophotometer (1100−200 nm). ^{1}H NMR spectra were recorded on a Bruker DPX400 spectrometer at 298 K. The residual ^{1}H present in DMSO-d_6 was used as internal reference. The assignment was proven by 2D NMR (^{13}C,^{1}H; ^{1}H,^{1}H, and ^{13}C,^{1}H via long-range couplings) spectra. Abbreviations for NMR data are: py = pyridine, pz = pyrazine, $C_{q,py}$ = quaternary carbon of pyridine, $C_{q,pz}$ = quaternary carbon of pyrazine. EPR measurements were performed on a Bruker ElexSys E500 EPR-spectrometer equipped with an EPR-910 Oxford Instruments helium-flow cryostat or on a Bruker ESP300E spectrometer in a quartz-Dewar filled with liquid nitrogen. An average spin concentration was calculated by comparison with a mouse R2 standard with a well-known radical content calibrated earlier against the copper standard.

Syntheses of Complexes. 2-Acetylpyridine *N,N*-Dimethylthiosemicarbazonato-*N,N,S*-dichlorogallium(III), $Ga(L^1)Cl_2$ (6). To 2-acetylpyridine *N,N*-dimethylthiosemicarbazone (**1**) (0.60 g, 2.70 mmol) in boiling dry ethanol (22 mL) was added an ethanolic gallium(III) chloride solution (2.29 mmol/mL) (0.59 mL, 1.35 mmol). After a few minutes, a yellow precipitate was formed. The reaction mixture was heated at 90 °C for 1 h. The product was separated from the hot solution by filtration, washed with dry ethanol, and dried *in vacuo*. Yield: 0.33 g (68%). Anal. ($C_{10}H_{13}Cl_2GaN_4S$): C, H, N. ^1H and ^{13}C NMR, mass spectrometry, IR and UV−vis spectroscopy data for **6** and all following complexes can be found in Supporting Information. Crystals suitable for X-ray data collection were obtained from chloroform saturated with *n*-hexane.

2-Acetylpyridine *N*-Pyrrolidinylthiosemicarbazonato-*N,N,S*-dichlorogallium(III), $Ga(L^2)Cl_2$ (7). To 2-acetylpyridine *N*-pyrrolidinylthiosemicarbazone (**2**) (0.30 g, 1.21 mmol) in dry ethanol (24 mL) at 75 °C was added an ethanolic gallium(III) chloride solution (3.13 mmol/mL) (0.77 mL, 2.42 mmol) dropwise within 3 min. The reaction mixture was cooled down to room temperature and stirred overnight. The reaction mixture was allowed to stand at 4 °C for 1 h, and the yellow precipitate was filtered off, washed with dry ethanol, and dried *in vacuo*. Yield: 0.38 g (82%). Anal. ($C_{12}H_{15}Cl_2GaN_4S$): C, H, N, S. Crystals suitable for X-ray data collection were obtained from ethanol/chloroform 1:2 solution saturated with diethyl ether.

[Bis(2-acetylpyridine *N,N*-dimethylthiosemicarbazonato)-*N,N,S*-gallium(III)] Hexafluorophosphate, $[Ga(L^1)_2]PF_6$ (8). To 2-acetylpyridine *N,N*-dimethylthiosemicarbazone (**1**) (0.20 g, 0.90 mmol) in dry ethanol (20 mL) was added gallium(III) nitrate nonahydrate (0.19 g, 0.45 mmol) in ethanol (5 mL), and the mixture was stirred for 15 min at room temperature until all ligand had dissolved. Addition of ammonium hexafluorophosphate (0.29 g, 1.80 mmol) produced a yellow precipitate. The reaction mixture was stirred further for 30 min at room temperature. The precipitate was filtered off, washed with ethanol, and dried *in vacuo*. Yield: 0.27 g (91%). Anal. ($C_{20}H_{26}F_6GaN_8PS_2$): C, H, N.

[Bis(2-acetylpyridine *N*-pyrrolidinylthiosemicarbazonato)-*N,N,S*-gallium(III)] Hexafluorophosphate, $[Ga(L^2)_2]PF_6$ (9). To 2-acetylpyridine *N*-pyrrolidinylthiosemicarbazone (**2**) (0.70 g, 2.82 mmol) in dry ethanol (70 mL) was added gallium(III) nitrate nonahydrate (0.59 g, 1.41 mmol) in dry ethanol (14 mL) at 50 °C. The reaction mixture was stirred for 1 h and then cooled down to room temperature with an ice bath. To the clear yellow solution was added ammonium hexafluorophosphate (0.23 g, 1.40 mmol) in dry ethanol (14 mL) in one portion. The reaction mixture was stirred for 30 min at room temperature and then cooled below 5 °C with an ice bath. The yellow precipitate formed was filtered off and washed with dry ethanol. The crude product was recrystallized from methanol (100 mL) and dried *in vacuo* at 50 °C. Yield: 0.77 g (77%). Anal. ($C_{24}H_{30}F_6GaN_8PS_2$): C, H, N, S.

[Bis(acetylpyrazine *N,N*-dimethylthiosemicarbazonato)-*N,N,S*-gallium(III)] Hexafluorophosphate, $[Ga(L^3)_2]PF_6$ (10). To acetylpyrazine *N,N*-dimethylthiosemicarbazone (**3**) (0.30 g, 1.34 mmol) in ethanol (30 mL) at room-temperature was added gallium(III) nitrate nonahydrate (0.28 g, 0.67 mmol) in ethanol (9 mL) and stirred for 15 min until all ligand had dissolved. After the addition of ammonium hexafluorophosphate (0.44 g, 2.68 mmol), an orange solid formed. The precipitate was filtered off, washed with ethanol, and dried *in vacuo*. Yield: 0.40 g (90%). Anal. ($C_{18}H_{24}F_6GaN_{10}PS_2$): C, H, N. Crystals suitable for X-ray data collection were obtained from chloroform saturated with *n*-hexane.

[Bis(acetylpyrazine *N*-pyrrolidinylthiosemicarbazonato)-*N,N,S*-gallium(III)] Hexafluorophosphate, $[Ga(L^4)_2]PF_6$ (11). To acetylpyrazine *N*-pyrrolidinylthiosemicarbazone (**4**) (0.50 g, 2.00 mmol) in dry ethanol (50 mL) at 50 °C was added gallium(III) nitrate nonahydrate (0.42 g, 1.00 mmol) in ethanol (10 mL). The reaction mixture was stirred for 30 min and then cooled down to room temperature with an ice bath. To the clear yellow solution was added ammonium hexafluorophosphate (0.16 g, 1.00 mmol) in dry ethanol (10 mL). The reaction mixture was stirred for 2 h at room temperature and then allowed to stand at 4 °C overnight. The orange precipitate formed was filtered off, washed with dry ethanol, and dried *in vacuo*. Yield: 0.40 g (56%). Anal. ($C_{22}H_{28}F_6GaN_{10}PS_2$): C, H, N, S. Crystals suitable for X-ray data collection were obtained from chloroform saturated with *n*-hexane.

[Bis(acetylpyrazine *N*-piperidinylthiosemicarbazonato)-*N,N,S*-gallium(III)] Hexafluorophosphate, $[Ga(L^5)_2]PF_6$ (12). To acetylpyrazine *N*-piperidinylthiosemicarbazone (**5**) (0.32 g, 1.16 mmol) in dry ethanol (30 mL) at 50 °C was added gallium(III) nitrate nonahydrate (0.24 g, 0.58 mmol) in ethanol (6 mL). The reaction mixture was stirred for 40 min and then cooled down to room temperature with an ice bath. To the clear orange solution was added ammonium hexafluorophosphate (0.10 g, 0.61 mmol) in dry ethanol (6 mL). The reaction mixture was allowed to stand at 4 °C for 1.5 h. The orange precipitate was filtered off, washed with dry ethanol, and dried *in vacuo*. Yield: 0.25 g (57%). Anal. ($C_{24}H_{32}F_6GaN_{10}PS_2$): C, H, N, S.

[Bis(2-acetylpyridine *N,N*-dimethylthiosemicarbazonato)-*N,N,S*-iron(III)] Tetrachloroferrate(III), $[Fe(L^1)_2][FeCl_4]$ (13). The complex has been prepared following the literature protocol.[35] Crystals suitable for X-ray data collection were obtained from chloroform saturated with *n*-hexane.

[Bis(2-acetylpyridine *N*-pyrrolidinylthiosemicarbazonato)-*N,N,S*-iron(III)] Tetrachloroferrate(III), $[Fe(L^2)_2][FeCl_4]$ (14). To 2-acetylpyridine *N*-pyrrolidinylthiosemicarbazone (**2**) (0.20 g, 0.80 mmol) in dry ethanol (24 mL) at 70 °C was added an ethanolic iron(III) chloride solution (0.26 mmol/mL) (3.1 mL, 0.80 mmol). The reaction mixture was stirred for 30 min, cooled down to room temperature, and then allowed to stand at 4 °C overnight. The black precipitate was filtered off, washed with dry ethanol, and dried *in vacuo*. Yield: 0.13 g (43%). Anal. ($C_{24}H_{30}Cl_4Fe_2N_8S_2$): C, H, N, S.

[Bis(acetylpyrazine *N,N*-dimethylthiosemicarbazonato)-*N,N,S*-iron(III)] Tetrachloroferrate(III), $[Fe(L^3)_2][FeCl_4]$ (15). To acetylpyrazine *N,N*-dimethylthiosemicarbazone (**3**) (0.23 g, 1.03 mmol) in boiling dry ethanol (15 mL) was added an ethanolic iron(III) chloride solution (0.17 mmol/mL) (6 mL, 1.03 mmol). The reaction mixture was refluxed for 30 min and cooled down to room temperature. The black precipitate was filtered off, washed with absolute ethanol, and dried *in vacuo*. Yield: 0.21 g (57%). Anal. ($C_{18}H_{24}Cl_4Fe_2N_{10}S_2$): C, H, N. Crystals suitable for X-ray data collection were obtained from chloroform saturated with *n*-hexane.

[Bis(acetylpyrazine *N*-pyrrolidinylthiosemicarbazonato)-*N,N,S*-iron(III)] Tetrachloroferrate(III), $[Fe(L^4)_2][FeCl_4]$ (16). To acetylpyrazine *N*-pyrrolidinylthiosemicarbazone (**4**) (0.30 g, 1.20 mmol) in dry ethanol (30 mL) at 70 °C was added an ethanolic iron(III) chloride solution (0.12 mmol/mL) (10 mL, 1.20 mmol). The reaction mixture was stirred for 30 min and cooled down to room temperature, and a second portion of an ethanolic iron(III) chloride solution (0.12 mmol/mL) (5 mL, 0.60 mmol) was added. The reaction mixture was allowed to stand at 4 °C for 45 min. The black precipitate formed was filtered off, washed with dry ethanol, and dried *in vacuo*. Yield: 0.41 g (90%). Anal. ($C_{22}H_{28}Cl_4Fe_2N_{10}S_2$): C, H, N, S. Crystals suitable for X-ray data collection were obtained from chloroform saturated with *n*-hexane.

[Bis(acetylpyrazine *N*-piperidinylthiosemicarbazonato)-*N,N,S*-iron(III)] Tetrachloroferrate(III), $[Fe(L^5)_2][FeCl_4]$ (17). To acetylpyrazine *N*-piperidinylthiosemicarbazone (**5**) (0.32 g, 1.16 mmol) in dry ethanol (30 mL) at 70 °C was added an ethanolic iron(III) chloride solution (0.12 mmol/mL) (5 mL, 0.60 mmol). The reaction mixture was stirred for 40 min and then cooled down to room temperature. An ethanolic iron(III) chloride solution (0.12 mmol/mL) (10 mL, 1.20 mmol) was added again in one portion, leading to the precipitation of the product. The reaction mixture was allowed to stand at 4 °C for 1 h. The black precipitate was filtered off, washed with dry ethanol, and dried *in vacuo*. Yield: 0.41 g (88%). Anal. ($C_{24}H_{32}Cl_4Fe_2N_{10}S_2$): C, H, N, S. Crystals suitable for X-ray data collection were obtained from chloroform saturated with *n*-hexane.

[Bis(2-acetylpyridine *N,N*-dimethylthiosemicarbazonato)-*N,N,S*-iron(III)] Hexafluorophosphate, $[Fe(L^1)_2]PF_6$ (18). To

2-acetylpyridine *N*,*N*-dimethylthiosemicarbazone (**1**) (0.30 g, 1.35 mmol) in ethanol (15 mL), iron(III) nitrate nonahydrate (0.27 g, 0.67 mmol) in ethanol (5 mL) was added at room temperature. To the black solution formed was added ammonium hexafluorophosphate (0.44 g, 2.70 mmol) in ethanol (5 mL), and the mixture was stirred at room temperature for 1.5 h and subsequently refluxed for 1 h. After the reaction mixture cooled down to room temperature, the black precipitate was filtered off, washed with ethanol, and dried *in vacuo*. Yield: 0.32 g (72%). Anal. ($C_{20}H_{26}F_6FeN_8PS_2$): C, H, N. Crystals suitable for X-ray data collection were obtained from chloroform saturated with *n*-hexane.

[Bis(2-acetylpyridine *N*-pyrrolidinylthiosemicarbazonato)-*N*,*N*,*S*-iron(III)] Hexafluorophosphate, [Fe(L^2)$_2$]PF$_6$ (19). To 2-acetylpyridine *N*-pyrrolidinylthiosemicarbazone (**2**) (0.70 g, 2.82 mmol) in dry ethanol (70 mL) at 70 °C was added iron(III) nitrate nonahydrate (0.57 g, 1.41 mmol) in dry ethanol (15 mL). The reaction mixture was stirred for 30 min and cooled down to room temperature with an ice bath. To the clear dark solution was added ammonium hexafluorophosphate (0.23 g, 1.41 mmol) in dry ethanol (14 mL). The reaction mixture was stirred for 30 min at room temperature and then allowed to stand at 4 °C overnight. The black precipitate was filtered off, recrystallized from methanol (100 mL), and dried *in vacuo* at 50 °C. Yield: 0.88 g (91%). Anal. ($C_{24}H_{30}F_6FeN_8PS_2$): C, H, N, S.

[Bis(acetylpyrazine *N*,*N*-dimethylthiosemicarbazonato)-*N*,*N*,*S*-iron(III)] Hexafluorophosphate, [Fe(L^3)$_2$]PF$_6$ (20). To acetylpyrazine *N*,*N*-dimethylthiosemicarbazone (**3**) (0.30 g, 1.34 mmol) in ethanol (40 mL) was added iron(III) nitrate nonahydrate (0.27 g, 0.67 mmol) in ethanol (5 mL). The reaction mixture was stirred at room temperature for 30 min and filtered. The black precipitate formed after the addition of ammonium hexafluorophosphate (0.44 g, 2.70 mmol) was stirred at room temperature for 1 h, filtered off, washed with ethanol, and dried *in vacuo*. Yield: 0.40 g (92%). Anal. ($C_{18}H_{24}F_6FeN_{10}PS_2$): C, H, N.

[Bis(acetylpyrazine *N*-pyrrolidinylthiosemicarbazonato)-*N*,*N*,*S*-iron(III)] Hexafluorophosphate, [Fe(L^4)$_2$]PF$_6$ (21). To acetylpyrazine *N*-pyrrolidinylthiosemicarbazone (**4**) (0.30 g, 1.20 mmol) in dry ethanol (30 mL) at 70 °C was added iron(III) nitrate nonahydrate (0.24 g, 0.60 mmol) in ethanol (6 mL). The reaction mixture was stirred for 30 min and then cooled down to room temperature with an ice bath. To the clear dark solution was added ammonium hexafluorophosphate (0.10 g, 0.61 mmol) in dry ethanol (6 mL). The reaction mixture was stirred for 1.5 h at room temperature and then allowed to stand at 4 °C overnight. The black precipitate was filtered off, washed with dry ethanol, and dried *in vacuo*. Yield: 0.37 g (89%). Anal. ($C_{22}H_{28}F_6FeN_{10}PS_2$): C, H, N, S. Crystals suitable for X-ray data collection were obtained from chloroform saturated with *n*-hexane.

[Bis(acetylpyrazine *N*-piperidinylthiosemicarbazonato)-*N*,*N*,*S*-iron(III)] Hexafluorophosphate, [Fe(L^5)$_2$]PF$_6$ (22). To acetylpyrazine *N*-piperidinylthiosemicarbazone (**5**) (0.32 g, 1.16 mmol) in dry ethanol (30 mL) at 70 °C was added iron(III) nitrate nonahydrate (0.24 g, 0.60 mmol) in ethanol (6 mL). The reaction mixture was stirred for 30 min and then cooled down to room temperature with an ice bath. To the clear dark solution was added ammonium hexafluorophosphate (0.10 g, 0.61 mmol) in dry ethanol (6 mL). The reaction mixture was stirred at room temperature for 3 h. The black precipitate was filtered off, washed with dry ethanol, and dried *in vacuo*. Yield: 0.39 g (90%). Anal. ($C_{24}H_{32}F_6FeN_{10}PS_2$): C, H, N, S.

Crystallographic Structure Determination. X-ray diffraction measurements were performed on a Nonius Kappa CCD and a Bruker X8APEX II CCD-diffractometer. Details of the structure determination are given in Table S2.

Crystal data, data collection parameters, and structure refinement details for **6**, **10**, **11**, **13**, **15**−**18**, and **21** are given in Tables S2−S4. The structures were solved by direct methods and refined by full-matrix least-squares techniques. Non-hydrogen atoms were refined with anisotropic displacement parameters. H atoms were placed at calculated positions and refined as riding atoms in the subsequent least-squares model refinements. The isotropic thermal parameters were estimated to be 1.2 times the values of the equivalent isotropic thermal parameters of the atoms to which hydrogens were bonded. The following computer programs were used: structure solution, SHELXS-97;[48] refinement, SHELXL-97;[49] molecular diagrams, ORTEP;[50] computer: Pentium IV; scattering factors.[51] Crystallographic data have been deposited with the Cambridge Crystallographic Data Center with numbers CCDC603767-603775. Copies of data can be obtained, free of charge, on application to CCDC, 12 Union Road, Cambridge CB2 1EZ, U.K. (deposit@ccdc.com.ac.uk).

Cell Lines and Culture Conditions. Human 41M (ovarian carcinoma) and SK-BR-3 (mammary carcinoma) cells were kindly provided by Lloyd R. Kelland (CRC Centre for Cancer Therapeutics, Institute of Cancer Research, Sutton, UK) and Evelyn Dittrich (General Hospital, Medical University of Vienna, Austria), respectively. Cells were grown in 75 cm^2 culture flasks (Iwaki) as adherent monolayer cultures in complete culture medium, i.e., Minimal Essential Medium (MEM) supplemented with 10% heat-inactivated fetal bovine serum, 1 mM sodium pyruvate, 4 mM L-glutamine, and 1% nonessential amino acids (100×) (all purchased from Gibco/Invitrogen). Cultures were maintained at 37 °C in a humidified atmosphere containing 5% CO_2.

Cytotoxicity Tests in Cancer Cell Lines. Cytotoxicity was determined by means of a colorimetric microculture assay (MTT assay, MTT = 3-(4,5-dimethyl-2-thiazolyl)-2,5-diphenyl-2*H*-tetrazolium bromide). 41M and SK-BR-3 cells were harvested from culture flasks by trypsinization and seeded into 96-well microculture plates (Iwaki). A cell density of 4×10^3 cells/well was chosen in order to ensure exponential growth throughout drug exposure. After a 24 h preincubation, cells were exposed to solutions of the test compounds in 200 μL/well complete culture medium for 96 h. For this purpose, the compounds were dissolved in DMSO and then serially diluted in complete culture medium such that the effective DMSO content did not exceed 0.5%. At the end of exposure, drug solutions were replaced by 100 μL/well RPMI1640 culture medium (supplemented with 10% heat-inactivated fetal bovine serum) plus 20 μL/well MTT solution in phosphate-buffered saline (5 mg/mL PBS). After incubation for 4 h, the medium/MTT mixtures were removed, and the formazan crystals formed by the mitochondrial dehydrogenase activity of vital cells were dissolved in 150 μL DMSO per well. Optical densities at 550 nm were measured with a microplate reader (Tecan Spectra Classic), using a reference wavelength of 690 nm in order to correct for unspecific absorption. The quantity of vital cells was expressed in terms of T/C values by comparison to untreated control microcultures, and IC_{50} values were calculated from concentration-effect curves by interpolation. Evaluation is based on means from at least three independent experiments, each comprising six microcultures per concentration level. Differences between cytotoxic potencies of the uncomplexed ligands and their gallium(III) and iron(III) complexes were analyzed using the Wilcoxon rank sum test.[52]

Quenching of the Tyrosyl Radical of Mouse Ribonucleotide Reductase R2 Protein. Highly purified mouse ribonucleotide reductase R2 protein[44] was used for incubation with ligand **1** and its gallium(III) and iron(III) complexes **8** and **18**, correspondingly, as well as $Ga(NO_3)_3$ and $Fe(NO_3)_3$.

Ligand **1** and complexes **8** and **18** are well soluble in DMSO but only sparingly soluble in water. The final DMSO concentration in the protein solution was kept at 1.1%. The solubility of $Ga(NO_3)_3$ and $Fe(NO_3)_3$ in DMSO was tested and found to be below the mM range. Thus, $Ga(NO_3)_3$ and $Fe(NO_3)_3$ were dissolved in water. A concentrated solution of reconstituted mouse ribonucleotide reductase R2 protein was diluted to 30 μM R2 monomer in buffer (50 mM Tris/HCl, pH 7.6, and 100 mM KCl in H_2O). This solution should contain 12−21 μM tyrosyl radical (Y*) depending on the yield of the reconstitution. Solutions each containing 3 mM 2-acetylpyridine *N*,*N*-dimethylthiosemicarbazone (**1**), [Ga(L^1)$_2$][PF$_6$] (**8**), or [Fe(L^1)$_2$][PF$_6$] (**18**) in DMSO and $Ga(NO_3)_3$ or $Fe(NO_3)_3$ in water were prepared. Six samples were prepared by mixing 180 μL of 30 μM R2 monomer (15 μM R2) solution with each of the following: 2 μL of DMSO, 2 μL of 3 mM **1** in DMSO, 2 μL of 3

mM **8** in DMSO, 2 μL of 3 mM **18** in DMSO, 2 μL of 3 mM $Ga(NO_3)_3$ in water and 2 μL of DMSO, and 2 μL of 3 mM $Fe(NO_3)_3$ in water and 2 μL of DMSO in Eppendorf reaction vials and transferring them into 4 mm outer diameter quartz-glass EPR tubes. After a total incubation time of 10 and 40 min at 298 K, they were frozen slowly in liquid nitrogen, and EPR spectra were measured at 40 K. As dilution was negligible here, this yielded a 1:1 molar ratio of R2 monomer and the tested compound (30−33 μM each). The same operations were repeated twice in the presence of 1 mM dithiothreitol with 15 min and >16 h incubation time at 298 K.

A second series of samples were prepared in an anaerobic tent. The buffer solution as well as the other stable solutions (3 mM each of **1**, **8**, and **18** in DMSO and $Ga(NO_3)_3$ and $Fe(NO_3)_3$ in H_2O) were bubbled with argon for 30 min. They were degassed by the vacuum applied in the lock of the anaerobic tent and left standing open for equilibration inside the tent for more then 16 h. The concentrated protein solution was degassed with great care in the lock and diluted 40-fold with the anaerobic buffer. The 20 mM DTT solution was prepared freshly inside the tent from preweighed powder and anaerobic buffer. Solutions were mixed in Eppendorf reaction vials and transferred to the bottom of an EPR tube by a Hamilton syringe with a long needle. EPR tubes were sealed with stoppers made from butyl-rubber and frozen immediately in liquid nitrogen. As indicated by the aerobic results, DTT is starting the reaction, so all other compounds were mixed with the 30 μM R2 monomer solution in advance. The time for addition of DTT, transfer to the EPR tube, and freezing it was estimated to take about 1 min; thus, the first time point is set to 1 min. The EPR spectra were measured at 77 K. Three types of blanks were prepared: (i) 30 μM R2 monomer; (ii) 30 μM R2 monomer in 1% DMSO; (iii) 30 μM R2 monomer in 1% DMSO and 1 mM DTT. For the other five samples, final concentrations were 30 μM R2 monomer, 1% DMSO, 30 μM reactive species, and 1 mM DTT.

Acknowledgment. The authors are indebted to the FWF (Austrian Science Fund), to the Austrian Council for Research and Technology Development, COST (European Cooperation in the Field of Scientific and Technical Research), Prof. Dr. W. Lubitz and the Max Planck Institute for Bioinorganic Chemistry, Mülheim an der Ruhr, Germany, and Faustus Forschung Austria, Translational Drug Development AG, Vienna, Austria, for financial support. We also thank Dr. Markus Galanski for NMR measurements, Dr. Alexey Nazarov and Peter Unteregger for mass spectra measurements, Prof. Gerald Giester for collection of X-ray data for compounds **6**, **10**, **11**, **13**, **15**−**17**, and **21**, and G. Schmitz for cell growth and purification of mouse R2 protein.

Supporting Information Available: Spectroscopic data [^{1}H and ^{13}C NMR spectra, mass spectra, IR, and UV−vis spectra (Figures S1−S4)], microanalytical data, results of kinetic measurements, crystallographic data, details of X-ray data collection and refinement, and the results of X-ray diffraction studies of **6**, **10**, **11**·$CHCl_3$, **13**, **15**, **16**·$CHCl_3$, **17**·$CHCl_3$, **18**, and **21** (Figures S5−S10). This material is available free of charge via the Internet at http://pubs.acs.org.

References

(1) Brockman, R. W.; Thomson, J. R.; Bell, M. J.; Skipper, H. E. Observations on the antileukemic activity of pyridine-2-carboxaldehyde thiosemicarbazone and thiocarbohydrazone. *Cancer Res.* **1956**, *16*, 167−170.

(2) West, D. X.; Padhye, S. B.; Sonawane, P. B. Structural and physical correlations in the biological properties of transition metal heterocyclic thiosemicarbazone and *S*-alkyldithiocarbazate complexes. *Struct. Bond.* **1991**, *76*, 1−50.

(3) Moore, E. C.; Zedeck, M. S.; Agrawal, K. C.; Sartorelli, A. C. Inhibition of ribonucleoside diphosphate reductase by 1-formylisoquinoline thiosemicarbazone and related compounds. *Biochemistry* **1970**, *9*, 4492−4498.

(4) Brockman, R. W.; Sidwell, R. W.; Arnett, G.; Shaddix, S. Heterocyclic thiosemicarbazones: correlation between structure, inhibition of ribonucleotide reductase, and inhibition of DNA viruses. *Proc. Soc. Exp. Biol. Med.* **1970**, *133*, 609−614.

(5) French, F. A.; Blanz, E. J., Jr.; Shaddix, S. C.; Brockman, R. W. α-(*N*)-Formylheteroaromatic thiosemicarbazones. Inhibition of tumor-derived ribunucleoside diphosphate reductase and correlation with in vivo antitumor activity. *J. Med. Chem.* **1974**, *17*, 172−181.

(6) Moore, E. C.; Sartorelli, A. C. Inhibition of ribonucleotide reductase by α-(*N*)-heterocyclic carboxaldehyde thiosemicarbazones. *Pharm. Ther.* **1984**, *24*, 439−447.

(7) Agrawal, K. C.; Sartorelli, A. C. The chemistry and biological activity of α-(*N*)-heterocyclic carboxaldehyde thiosemicarbazones. *Prog. Med. Chem.* **1978**, *15*, 321−356.

(8) Liu, M.-C.; Lin, T.-S.; Sartorelli, A. C. Chemical and biological properties of cytotoxic α-(*N*)-heterocyclic carboxaldehyde thiosemicarbazones. *Prog. Med. Chem.* **1995**, *32*, 1−35.

(9) Eklund, H.; Uhlin, U.; Farnegardh, M.; Logan, D. T.; Nordlund, P. Structure and function of the radical enzyme ribonucleotide reductase. *Prog. Biophys. Mol. Biol.* **2001**, *77*, 177−268.

(10) Saryan, L. A.; Ankel, E.; Krishnamurti, C.; Petering, D. H. Comparative cytotoxic and biochemical effects of ligands and metal complexes of α-*N*-heterocyclic carboxaldehyde thiosemicarbazones. *J. Med. Chem.* **1979**, *22*, 1218−1221.

(11) Preidecker, P. J.; Agrawal, K. C.; Sartorelli, A. C.; Moore, E. C. Effects of the ferrous chelate of 4-methyl-5-amino-1-formylisoquinoline thiosemicarbazone (MAIQ-1) on the kinetics of reduction of CDP by ribonucleotide reductase of the Novikoff tumor. *Mol. Pharmacol.* **1980**, *18*, 507−512.

(12) Antholine, W.; Knight, J.; Whelan, H.; Petering, D. H. Studies of 2-formylpyridine thiosemicarbazone and its iron and copper complexes with biological systems. *Mol. Pharmacol.* **1977**, *13*, 89−98.

(13) Borges, R. H. U.; Paniago, E.; Beraldo, H. Equilibrium and kinetic studies of iron(II) and iron(III) complexes of some α(N)-heterocyclic thiosemicarbazones. Reduction of the iron(III) complexes of 2-formylpyridine thiosemicarbazone and 2-acetylpyridine thiosemicarbazone by cellular thiol-like reducing agents. *J. Inorg. Biochem.* **1997**, *65*, 267−275.

(14) Thelander, L.; Gräslund, A. Mechanism of inhibition of mammalian ribonucleotide reductase by the iron chelate of 1-formylisoquinoline thiosemicarbazone. Destruction of the tyrosine free radical of the enzyme in an oxygen-requiring reaction. *J. Biol. Chem.* **1983**, *258*, 4063−4066.

(15) Chaston, T. B.; Lovejoy, D. B.; Watts, R. N.; Richardson, D. R. Examination of the antiproliferative activity of iron chelators: multiple cellular targets and different mechanism of action of triapine compared with desferrioxamine and the potent pyridoxal isonicotinoyl hydrazone analogue 311. *Clin. Cancer Res.* **2003**, *9*, 402−414.

(16) Karon, M.; Benedict, W. F. Chromatid breakage: differential effect of inhibitors of DNA synthesis during G_2 phase. *Science* **1972**, *178*, 62.

(17) Tsiftsoglou, A. S.; Hwang, K. M.; Agrawal, K. C.; Sartorelli, A. C. Strand scission of sarcoma 180 tumor cell DNA induced by 1-formylisoquinoline thiosemicarbazone. *Biochem. Pharmacol.* **1975**, *24*, 1631−1633.

(18) Miller, M. C., III; Bastow, K. F.; Stineman, C. N.; Vance, J. R.; Song, S. C.; West, D. X.; Hall, I. H. The cytotoxicity of 2-formyl and 2-acetyl-(6-picolyl)-^{4}*N*-substituted thiosemicarbazones and their copper(II) complexes. *Arch. Pharm. Pharm. Med. Chem.* **1998**, *331*, 121−127.

(19) Miller, M. C., III; Stineman, C. N.; Vance, J. R.; West, D. X.; Hall, I. H. The cytotoxicity of copper(II) complexes of 2-acetyl-pyridyl-^{4}N-substituted thiosemicarbazones. *Anticancer Res.* **1998**, *18*, 4131−4140.

(20) Miller, M. C., III; Stineman, C. N.; Vance, J. R.; West, D. X.; Hall, I. H. Multiple mechanisms for cytotoxicity induced by copper(II) complexes of 2-acetylpyrazine-*N*-substituted thiosemicarbazones. *Appl. Organomet. Chem.* **1999**, *13*, 9−19.

(21) DeConti, R. C.; Toftness, B. R.; Agrawal, K. C.; Tomchick, R.; Mead, J. A. R.; Bertino, J. R.; Sartorelli, A. C.; Creasey, W. A. Clinical and pharmacological studies with 5-hydroxy-2-formylpyridine thiosemicarbazone. *Cancer Res.* **1972**, *32*, 1455−1462.

(22) Krakoff, I. H.; Etcubanas, E.; Tan, C.; Mayer, K.; Bethune, V.; Burchenal, J. H. Clinical trial of 5-hydroxypicolinaldehyde thiosemicarbazone (5-HP; NSC-107392), with special reference to its iron-chelating properties. *Cancer Chemother. Rep.* **1974**, *58*, 207−212.

(23) Feun, L.; Modiano, M.; Lee, K.; Mao, J.; Marini, A.; Savaraj, N.; Plezia, P.; Almassian, B.; Colacino, E.; Fischer, J.; Mac Donald, S. Phase I and pharmacokinetic study of 3-aminopyridine-2-carboxaldehyde thiosemicarbazone (3-AP) using a single intravenous dose schedule. *Cancer Chemother. Pharmacol.* **2002**, *50*, 223−229.

(24) Giles, F. J.; Fracasso, P. M.; Kantarjian, H. M.; Cortes, J. E.; Brown, R. A.; Verstovsek, S.; Alvarado, Y.; Thomas, D. A.; Faderl, S.; Garcia-Manero, G.; Wright, L. P.; Samson, T.; Cahill, A.; Lambert, P.; Plunkett, W.; Sznol, M.; DiPersio, J. F.; Gandhi, V. Phase I and pharmacodynamic study of triapine, a novel ribonucleotide reductase inhibitor, in patients with advanced leukemia. *Leuk. Res.* **2003**, *27*, 1077−1083.

(25) Murren, J.; Modiano, M.; Clairmont, C.; Lambert, P.; Savaraj, N.; Doyle, T.; Sznol, M. Phase I and pharmacokinetic study of triapine, a potent ribonucleotide reductase inhibitor, administered daily for five days in patients with advanced solid tumors. *Clin. Cancer Res.* **2003**, *9*, 4092−4100.

(26) Wadler, S.; Makower, D.; Clairmont, C.; Lambert, P.; Fehn, K.; Sznol, M. Phase I and pharmacokinetic study of the ribonucleotide reductase inhibitor, 3-aminopyridine-2-carboxaldehyde thiosemicarbazone, administered by 96-hour intravenous continuous infusion. *J. Clin. Oncol.* **2004**, *22*, 1553−1563.

(27) Finch, R. A.; Liu, M.-C.; Grill, S. P.; Rose, W. C.; Loomis, R.; Vasquez, K. M.; Cheng, Y.-C.; Sartorelli, A. C. Triapine (3-aminopyridine-2-carboxaldehyde-thiosemicarbazone): a potent inhibitor of ribonucleotide reductase activity with broad spectrum of antitumor activity. *Biochem. Pharmacol.* **2000**, *59*, 983−991.

(28) Hedley, D. W.; Tripp, E. H.; Slowiaczek, P.; Mann, G. J. Effect of gallium on DNA synthesis by human T-cell lymphoblasts. *Cancer Res.* **1988**, *48*, 3014−3018.

(29) Bernstein, L. R. Mechanisms of therapeutic activity for gallium. *Pharmacol. Rev.* **1998**, *50*, 665−682.

(30) Collery, P.; Keppler, B.; Madoulet, C.; Desoize, B. Gallium in cancer treatment. *Crit. Rev. Oncol. Hematol.* **2002**, *42*, 283−296.

(31) Jakupec, M. A.; Keppler, B. K. Gallium in cancer treatment. *Curr. Top. Med. Chem.* **2004**, *4*, 1575−1583.

(32) Chitambar, C. R.; Narasimhan, J.; Guy, J.; Sem, D. S.; O'Brien, W. J. Inhibition of ribonucleotide reductase by gallium in murine leukemic L1210 cells. *Cancer Res.* **1991**, *51*, 6199−6201.

(33) Narasimhan, J.; Antholine, W. E.; Chitambar, C. R. Effect of gallium on the tyrosyl radical of the iron-dependent M2 subunit of ribonucleotide reductase. *Biochem. Pharmacol.* **1992**, *44*, 2403−2408.

(34) Arion, V. B.; Jakupec, M. A.; Galanski, M.; Unfried, P.; Keppler, B. K. Synthesis, structure, spectroscopic and in vitro antitumour studies of a novel gallium(III) complex with 2-acetylpyridine ^4N-dimethylthiosemicarbazone. *J. Inorg. Biochem.* **2002**, *91*, 298−305.

(35) West, D. X.; Lewis, N. C. Transition metal ion complexes of thiosemicarbazones derived from 2-acetylpyridine. Part 2. The ^{4}N-dimethyl derivative. *Transition Metal. Chem.* **1988**, *13*, 277−290.

(36) Addison, A. W.; Rao, T. N.; Reedijk, J.; Van Rijn, J.; Verschoor, G. C. Synthesis, structure, and spectroscopic properties of copper(II) compounds containing nitrogen-sulfur donor ligands: the crystal and molecular structure of aqua[1,7-bis(N-methylbenzimidazol-2′-yl)-2,6-dithiaheptane]copper(II) perchlorate. *J. Chem. Soc., Dalton Trans.* **1984**, *7*, 1349−1356.

(37) Kowol, C. R.; Arion, V. B.; Keppler, B. K. Unpublished results.

(38) Scovill, J. P.; Klayman, D. L.; Franchino, C. F. 2-Acetylpyridine thiosemicarbazones. 4. Complexes with transition metals as antimalarial and antileukemic agents. *J. Med. Chem.* **1982**, *25*, 1261−1264.

(39) Easmon, J.; Pürstinger, G.; Heinisch, G.; Roth, T.; Fiebig, H. H.; Holzer, W.; Jäger, W.; Jenny, M.; Hofmann, J. Synthesis, cytotoxicity, and antitumor activity of copper(II) and iron(II) complexes of ^4N-azabicyclo[3.2.2]nonane thiosemicarbazones derived from acyl diazines. *J. Med. Chem.* **2001**, *44*, 2164−2171.

(40) Easmon, J.; Heinisch, G.; Holzer, W.; Rosenwirth, B. Novel thiosemicarbazones derived from formyl- and acyldiazines: synthesis, effects on cell proliferation, and synergism with antiviral agents. *J. Med. Chem.* **1992**, *35*, 3288−3296.

(41) French, F. A.; Blanz, E. J., Jr. The carcinostatic activity of thiosemicarbazones of formyl heteroaromatic compounds. III. Primary correlation. *J. Med. Chem.* **1966**, *9*, 585−589.

(42) Cory, J. G.; Cory, A. H.; Rappa, G.; Lorico, A.; Liu, M.-C.; Lin, T.-S.; Sartorelli, A. C. Structure-function relationships for a new series of pyridine-2-carboxaldehyde thiosemicarbazones on ribonucleotide reductase activity and tumor cell growth in culture and in vivo. *Adv. Enzyme Regul.* **1995**, *35*, 55−68.

(43) Klayman, D. L.; Scovill, J. P.; Mason, C. J.; Bartosevich, J. F.; Bruce, J.; Lin, A. J. 2-Acetylpyridine thiosemicarbazones. 6. 2-Acetylpyridine and 2-butyrylpyridine thiosemicarbazones as antileukemic agents. *Arzneim.-Forsch./Drug Res.* **1983**, *33*, 909−912.

(44) Schmidt, P. P.; Rova, U.; Katterle, B.; Thelander, L.; Graslund, A. Kinetic evidence that a radical transfer pathway in protein R2 of mouse ribonucleotide reductase is involved in generation of the tyrosyl free radical. *J. Biol. Chem.* **1998**, *273*, 21463−21472.

(45) Schmidt, P. P. Unpublished results.

(46) Nyholm, S.; Thelander, L.; Gräslund, A. Reduction and loss of the iron center in the reaction of the small subunit of mouse ribonucleotide reductase with hydroxyurea. *Biochemistry* 1993, *32*, 11569−11574.

(47) Klayman, D. L.; Scovill, J. P.; Bartosevich, J. F.; Mason, C. J. 2-Acetylpyridine thiosemicarbazones. 2. N^4,N^4-disubstituted derivates as potential antimalarial agents. *J. Med. Chem.* **1979**, *22*, 1367−1373.

(48) Sheldrick, G. M. *SHELXS-97, Program for Crystal Structure Solution*; University Göttingen: Göttingen, Germany, 1997.

(49) Sheldrick, G. M. *SHELXL-97, Program for Crystal Structure Refinement*; University Göttingen: Göttingen, Germany, 1997.

(50) Johnson, G. K. *Report ORNL-5138*; Oak Ridge National Laboratory: Oak Ridge, TN, 1976.

(51) *International Tables for X-ray Crystallography*; Kluwer Academic Press: Dodrecht, The Netherlands, 1992; Vol. C, Tables 4.2.6.8 and 6.1.1.4.

(52) Hollander, M.; Wolfe, D. A. *Nonparametric statistical inference*, 1st ed.; John Wiley & Sons: New York, 1973; pp 68−75.

JM0612618